Rock magnetism of tiny exsolved magnetite in plagioclase from a Paleoarchean granitoid in the Pilbara craton

メタデータ	言語: eng
	出版者:
	公開日: 2022-09-01
	キーワード (Ja):
	キーワード (En):
	作成者:
	メールアドレス:
	所属:
URL	https://doi.org/10.24517/00067008

Rock magnetism of tiny exsolved magnetite in plagioclase from a Paleoarchean granitoid in the Pilbara craton

Yoichi Usui[1], Takazo Shibuya[2], Yusuke Sawaki[3], and Tsuyoshi Komiya[4]

[1]Department of Deep Earth Structure and Dynamics Research, Japan Agency for Marine-Earth Science and Technology, Yokosuka, Japan, [2]Laboratory for Ocean-Earth Life Evolution Research, Japan Agency for Marine-Earth Science and Technology, Yokosuka, Japan, [3]Department of Earth and Planetary Sciences, Tokyo Institute of Technology, Tokyo, Japan, [4]Department of Earth Science and Astronomy, University of Tokyo, Tokyo, Japan

Abstract Granitoids are widespread in Precambrian terranes as well as the Phanerozoic orogenic belts, but they have garnered little attention in paleomagnetic studies, because granitoids often contain abundant coarse-grained, magnetically unstable oxides. In this study, the first example of tiny, needle-shaped, exsolved oxides in plagioclase in a Paleoarchean granitoid is reported. The magnetic properties of single plagioclase crystals with the exsolved oxide inclusions have been studied to determine their paleomagnetic recording fidelity. Demagnetization experiments and hysteresis parameters indicate that the oxide inclusions are near stoichiometric magnetite and magnetically very stable. First-order reversal curve (FORC) diagrams reveal negligible magnetostatic interactions. Minimal interactions are also reflected by very efficient acquisition of anhysteretic remanent magnetization. Single plagioclase crystals exhibit strong magnetic remanence anisotropies, which require corrections to their paleodirectional and paleointensity data. Nonetheless, quantitative consideration of anisotropy tensors of the single plagioclase crystals indicates that the bias can be mitigated by properly averaging data from a few tens of single crystals. From the nonlinear thermoremanence acquisition of the plagioclase crystals, we estimate that the plagioclase crystals can reconstruct paleointensity up to 50 μT. Local metamorphic condition suggests that those magnetite may carry remanence of ~3.2 to 3.3 Ga. We suggest that exsolved magnetite in granitoids is potentially a suitable target for the study of the early history of the geomagnetic field, and prompt detailed microscopic investigations as well as paleomagnetic tests to constrain the age of remanence.

1. Introduction

Archean paleomagnetic records are needed to estimate the secular change in the geodynamo activity and crustal tectonics. Moreover, an early geomagnetic field is hypothesized to be related to the Earth's habitability [e.g., *Tarduno et al.*, 2014], and the oldest paleomagnetic record is actively being investigated [e.g., *Usui et al.*, 2009; *Tarduno et al.*, 2010]. To obtain Archean paleomagnetic records, good magnetic recorders that can preserve the natural paleomagnetic record for billions of years are of crucial importance. Generally, Archean terranes are divisible into granite-greenstone belts and high-grade granulite-gneiss belts [*Windley and Bridgwater*, 1971]. Both are composed of granitic plutons and mafic volcanic rocks, with subordinate amounts of metasediments. Mafic volcanic rocks are usually preferred in studies of Phanerozoic paleomagnetism, because of their stable magnetic remanence [e.g., *Dunlop and Özdemir*, 1997]; however, in Archean terranes, mafic rocks are usually altered and contain secondary magnetic minerals [e.g., *Yoshihara and Hamano*, 2004], preventing reliable determination of primary Archean paleomagnetism. Granitic rocks retain more primary compositions and fabrics than their coeval, often pillow-bearing, mafic volcanic rocks because the latter were submarine extrusives, whereas the former were impermeable intrusives. Unfortunately, the magnetic mineralogy of granitic rocks hinders paleomagnetic studies. The main oxide mineral in most granitic rocks is coarse-grained magnetite, which in general has low magnetic stability, because its internal magnetic structures take multidomain (MD) states [e.g., *Dunlop and Özdemir*, 1997]; thus, the coarse-grained magnetite in Archean granitic rocks is susceptible to magnetic overprint by younger remanence. Therefore, Archean granitic rocks are rarely used in paleomagnetic studies.

Tarduno et al. [2007] introduced a novel approach to the study of paleomagnetism of Archean granitoids. In their study of the ~3.2 Ga Kaap Valley granitoid pluton in the Barberton greenstone belt, they conducted

selective measurements of single microcline and quartz crystals without visible inclusions under a binocular microscope. On the basis of magnetic measurements, they concluded that some crystals appear to contain invisible, tiny magnetic minerals that may have been entrapped during magmatic crystal growth. By measuring those single silicate crystals, they obtained paleodirectional and paleointensity data without contributions from the coarse-grained magnetite in the rock matrix. The paleomagnetic directions obtained by *Tarduno et al*. [2007] were different from those previously estimated from conventional whole-rock measurements in the same pluton [*Layer et al*., 1996]. *Tarduno et al*. [2007] considered that the difference was due to a complex magnetic overprint in the magnetically unstable coarse-grained magnetite in the whole-rock samples, and emphasized that the selective paleomagnetic measurements of tiny, magnetically stable single domain (SD) to pseudo-SD (PSD) magnetic minerals enables estimation of the primary remanence in Archean rocks. Similar technique has been successfully applied to ∼3.44 Ga dacite in the Barberton greenstone belt and yielded the oldest robust paleointensity results based on thermoremanent magnetizations [*Usui et al*., 2009; *Tarduno et al*., 2010]. Despite these successes, no other paleomagnetic results have been reported from Archean granitoids using the single crystal approach, mainly because single silicate crystals with tiny entrapped magnetic inclusions usually have extremely low magnetization, close to the sensitivity limit of commercially available magnetometers. Consequently, Archean paleomagnetic record remains very sparse, and we do not even know how the field might have varied on 100 Ma time scales.

In some plutonic and metamorphic rocks, silicate minerals such as plagioclase and pyroxene contain tiny rods of exsolved magnetite [e.g., *Evans and McElhinny*, 1966; *Evans et al*., 1968; *Hargraves and Young*, 1969; *Fleet et al*., 1980; *Davies*, 1981; *Wenk et al*., 2011]. Plagioclase and pyroxene containing exsolved magnetite has relatively strong magnetizations so that single crystals can be routinely measured in currently available rock magnetometers [*Renne et al*., 2002; *Usui and Nakamura*, 2009]. In addition, silicate crystals with exsolved magnetite show high magnetic stability with SD-like characteristics [*Renne et al*., 2002; *Feinberg et al*., 2005; *Muxworthy and Evans*, 2013], including ideal (linear) behavior in Thellier-type paleointensity experiments [*Dunlop et al*., 2005]. Slow cooling of plutonic rocks may provide time-averaged signal. For paleointensity studies, slow cooling necessitates a correction [*Dodson and McClelland-Brown*, 1980; *Halgedahl et al*., 1980]. A recent study [*Usui*, 2013] indicates that exsolved magnetite exhibits the cooling rate effect which is predictable by theory [*Dodson and McClelland-Brown*, 1980; *Halgedahl et al*., 1980]. There are some uncertainties in the timing and temperature of the magnetite exsolution [*Feinberg et al*., 2005]. Nonetheless, such properties indicate that the plagioclase and pyroxene, with their exsolved magnetite, provide excellent paleomagnetic recorders. Indeed, whole-rock samples of anorthosites and gabbros whose magnetic properties are dominated by exsolved magnetites have yielded successful paleodirectional and paleointensity results [*Selkin et al*., 2008; *Muxworthy et al*., 2013; *Usui*, 2013]. Most paleomagnetic studies of exsolved magnetite have focused on anorthosites and gabbros, but the recent discovery of exsolved magnetite in plagioclases in a Cretaceous granitoid [*Usui et al*., 2006] suggests that even Archean granitoids contain exsolved magnetite. However, to date, no paleomagnetic study has been conducted on the exsolved magnetite in Archean granitoids.

The single silicate technique is a powerful way of reducing the contribution from magnetically unstable coarse-grained magnetite [*Tarduno et al*., 2006, 2007]; however, the interpretation of paleomagnetism of single silicate crystals with exsolved magnetite may be complicated by magnetic anisotropy. Individual grains of exsolved magnetite are usually in the form of elongated rods or blades, and their alignment is controlled by the crystallographic orientations of their host silicate [e.g., *Fleet et al*., 1980; *Sobolev*, 1990; *Feinberg et al*., 2004; *Wenk et al*., 2011]. These features will result in high magnetic remanence anisotropy that should introduce a bias in directional and paleointensity records [e.g., *Uyeda et al*., 1963; *Coe*, 1979; *Selkin et al*., 2000]. Using the directional dependence of magnetic hysteresis properties, *Gee and Meurer* [2002] inferred strong preferred orientation of exsolved magnetites within clinopyroxene crystals from oceanic gabbros. The remanence anisotropy tensors were determined for orthopyroxene [*Lagroix and Borradaile*, 2000; *Selkin et al*., 2014] and plagioclase single crystals [*Usui and Nakamura*, 2009; *Selkin et al*., 2014] using anhysteretic remanent magnetization (ARM). These studies reported extremely high remanence anisotropy ($P_j = 2 \sim 35$, where P_j is the *Jelinek* [1981] anisotropy degree). *Selkin et al*. [2014] measured anisotropy tensors for more than 20 single silicate crystals, and successfully modeled whole-rock magnetic anisotropy using the anisotropy of single silicate crystals and lattice orientations of the silicates. However, the paleomagnetic bias in single silicate crystals due to the magnetic anisotropy of exsolved magnetite has not yet been quantified. In

USUI ET AL.   113

this study, we report the occurrence and magnetic properties of exsolved magnetites within plagioclases in a Paleoarchean granitoid. In particular, we carefully determine the magnetic anisotropy tensor of single plagioclase crystals and discuss the bias due to their anisotropy.

2. Samples

The sample examined in this study is single rock piece of medium-grained granodiorites from the Mount Edgar Igneous Complex in the Pilbara craton (21°18.309′S, 120°6.242′). The sample belongs to the Boodallana Suite [*Sims and Carson*, 2001], which has a whole-rock Rb-Sr age of 3210 ± 90 Ma [*Collins and Gray*, 1990] and a zircon SHRIMP U-Pb age of 3304 ± 10 Ma [*Williams and Collins*, 1990]. It is presumed that the latter (~3300 Ma) represents the time of intrusion, while the former (~3200 Ma) represents the time of metamorphic reequilibration during the greenschist to lower amphibolite facies metamorphism [*Collins and Gray*, 1990]. The rocks appeared to have been emplaced and cooled in the late Paleoarchean, but note that the higher-potential metamorphic grade should have thermally reset any primary NRM. Also, the exsolution of magnetite within plagioclase may have occurred during metamorphism. The magnetization in these cases would be Mesoarchean in age. Future paleomagnetic studies using Mount Edgar Igneous Complex should provide some evidence such as paleomagnetic field tests to constrain the age of remanence. The samples consist mainly of quartz, plagioclase, hornblende, biotite, and a Fe-Ti oxide (Figures 1a and 1b). Large oxide grains occur as discrete crystals or inclusions in biotites (Figure 1b). Plagioclase crystals contain tiny rods of magnetite (Figures 1c–1e). The magnetite rods appear to exhibit four sets of elongation directions. Magnetites with one elongation direction (vertical in Figure 1e) is more numerous and finer. The typical width of these fine magnetites is less than 1 μm, and the typical length is a few μm. Magnetites with other elongation directions have typical width of a few μm and typical varying from a few μm to a few tens of μm. Note that the occurrence of exsolved magnetite may be local phenomena even in a rock suite [*Usui et al.*, 2006].

3. Experimental Methods

Plagioclase crystals were handpicked from crushed rock samples and sonicated in distilled water. Under a binocular microscope, we selected clean crystals without sever sericitization or large inclusions. Crystals with extreme shape anisotropy were also avoided to reduce possible bias in magnetic anisotropy measurements. The appearance of the crystals ranges from clear transparent to semitransparent with black clouding. The size is typically between 0.3 and 1 mm in size (Figure 1f). We then performed ARM demagnetization experiments, magnetic hysteresis measurements, ARM anisotropy measurements, and TRM and ARM acquisition measurements on the selected crystals. For comparison, magnetic properties of whole-rock samples were also examined.

3.1. ARM Demagnetization

ARM demagnetization experiments were undertaken to evaluate magnetic mineralogy and stability. The ARM was imparted on three single plagioclase crystals using an AF demagnetizer DEM95 (Natsuhara Giken Co. Ltd) with a peak alternating field of 150 mT and a DC field of 70 μT. Demagnetizations were conducted using progressive AF demagnetization, progressive thermal demagnetization, and low-temperature demagnetization techniques. The AF demagnetization experiments were performed using the DEM95 with three-axis sample tumbling. The thermal demagnetization experiments were carried out using a custom-made infrared heating apparatus (Thermo Riko Co. Ltd). A sample is placed in a quartz glass tube and set in a small heating chamber made of SiC. The heating chamber is placed inside a two-layer mu-metal shield. Infrared light is generated outside the shield and transmitted to the SiC chamber through a quartz rod, and the temperature is monitored using a Pt thermocouple placed inside the SiC chamber. For the low-temperature demagnetization experiments, samples were soaked in liquid nitrogen in a styrene foam container. The liquid nitrogen evaporated in about 20 min, and samples were left in the container overnight. The cooling-heating cycles were performed in a two-layer mu-metal shield. The remanence of the plagioclase crystals was measured using a SQUID magnetometer Model 760 (2G Enterprises). For whole-rock samples, we examined cores with 2.5 cm diameter and 2.2 cm height of the granitoids. The AF and low-temperature demagnetization experiments were performed in the same way as those for the plagioclase crystals. The thermal demagnetization experiments were carried out using a TDS-1 thermal demagnetizer.
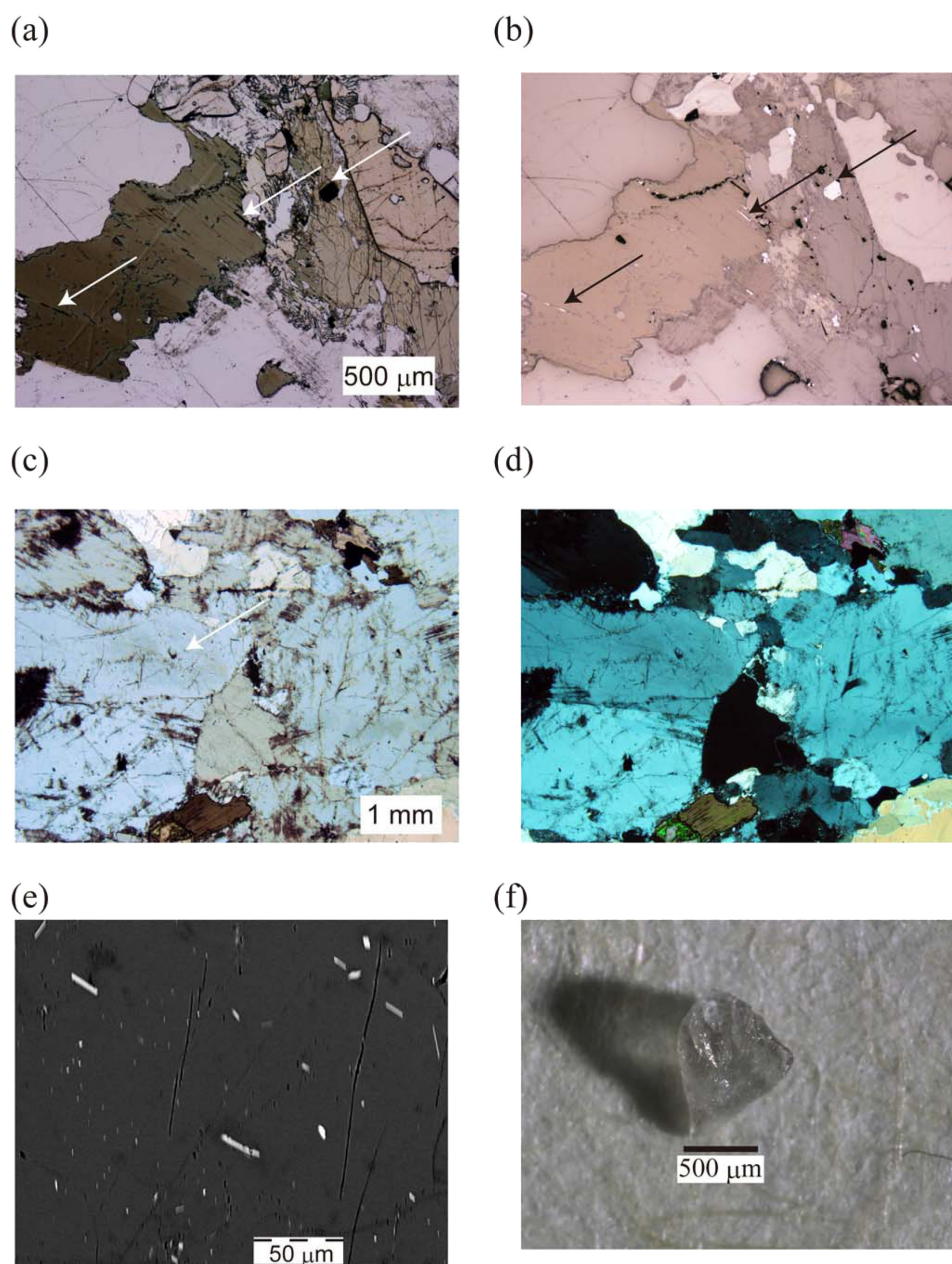
Figure 1. Microscope images of the studied granodiorite samples, highlighting the various occurrences of magnetic minerals. (a and b) Open-polarized and cross-polarized images. Arrows indicate oxides as discrete grains and grains along fractures in biotite (lower left). (c and d) Open-polarized and cross-polarized images of a plagioclase crystal containing exsolved magnetite. Arrow indicates the region with exsolved magnetite. (e) Backscatter electron image of exsolved magnetites. (f) Optical photomicrograph of typical plagioclase crystal used in rock magnetic measurements.

The remanence of the whole-rock samples was measured using an ASPIN spinner magnetometer (Natsuhara Giken Co. Ltd.).

3.2. Magnetic Hysteresis

Magnetic hysteresis measurements were performed to evaluate magnetic domain states and magnetostatic interactions. Conventional hysteresis parameters (saturation magnetization M_s; saturation remanence M_{rs}; coercivity H_c; and coercivity of remanence H_{cr}) and first-order reversal curves (FORCs) were determined using an alternating gradient field magnetometer (AGFM; Princeton Measurement Inc.) at the National Institute of Advanced Industrial Science and Technology, Tsukuba, Japan. The hysteresis parameters were

determined for 28 single plagioclase crystals. FORCs were measured for an assemblage of six plagioclase crystals to mitigate the potential effect of magnetic anisotropy. FORCs were analyzed [*Pike et al.*, 1999; *Roberts et al.*, 2000] using software FORCinel version 2.1 [*Harrison and Feinberg*, 2008]. For the whole-rock sample, a powder of ∼0.1 g was measured using a vibrating sample magnetometer (VSM; Princeton Measurement Inc.).

3.3. Remanence Anisotropy

Magnetic remanence anisotropy tensors were estimated based on the ARM of 40 single plagioclase crystals. We imparted ARMs along seven directions [*Nye*, 1957; *Borradaile and Stupavsky*, 1995] using the DEM95 with custom-made holders. The peak AF field was 150 mT and the DC field was 70 μT. All three components of a remanence vector were measured using the SQUID magnetometer and the anisotropy tensors were estimated through least squares fitting.

3.4. TRM and ARM Acquisition

TRM acquisition experiments were performed on four assemblages of plagioclases, each consisting of seven crystals. The TRM was imparted with the described custom-made infrared heating apparatus with peak temperature of 610°C. Applied DC fields were 20 and 10 μT, and then incremented from 30 to 100 μT at 10 μT steps. The extent of alteration due to the heating was checked by repeating TRM acquisitions at 20 μT after finishing all heating steps. After the TRM acquisition experiments, ARM acquisition experiments were performed on the same samples. The ARM was imparted using the DEM95. The peak AF field was 150 mT, and the DC bias field was incremented from 10 to 100 μT at 10 μT steps. We examined ARM acquisition of a 2.5 cm core sample for the whole-rock sample.

4. Results

4.1. ARM Demagnetization

Thermal demagnetization of ARM of the plagioclase crystals (Figure 2a) revealed a narrow unblocking temperature range; about 60% of the ARM was demagnetized between 525 and 585°C. The remanences were completely unblocked at 585°C. AF demagnetization revealed that the median destructive field (MDF) of ARM is ∼30 mT (Figure 2b). Note that the tumbling AF demagnetization used in this study is generally more effective in erasing remanence than the static three-axis AF demagnetization used in some previous studies [e.g., *Renne et al.*, 2002]. Low-temperature demagnetization erased ∼20% of the total ARM, similar to the effectiveness for the Lambertville plagioclase [*Halgedahl and Jarrard*, 1995].

The whole-rock sample has different demagnetization characteristics from the plagioclase crystals (Figures 2c and 2d). Compared with the plagioclase crystals, the whole-rock sample exhibits a broader unblocking temperature range, lower MDF of ∼15 mT, and larger remanence loss during the low-temperature demagnetization (∼50% of the total ARM). Those results show that the ARM of the whole-rock sample is mainly carried by coarse-grained magnetites.

4.2. Magnetic Hysteresis

Figure 3 shows the hysteresis parameters plotted on a Day plot [*Day et al.*, 1977; *Dunlop*, 2002]. The data are distributed in the SD and PSD regions. Two samples exhibit $M_{rs}/M_s > 0.5$. Those values are not expected for randomly oriented uniaxial particles, indicating that the observed hysteresis parameters are influenced by magnetic anisotropy of the plagioclase crystals, as demonstrated by *Gee and Meurer* [2002] for crystals from oceanic gabbros. At the same time, the data follow the standard SD-MD mixing curve [*Dunlop*, 2002], indicating that some exsolved magnetites are in a MD state. We obtained $M_{rs}/M_s = 0.32$ and $H_{cr}/H_c = 1.73$ by averaging the data from 28 grains.

The FORC diagrams are shown in Figure 4. The horizontal axis (H_c) reflects the coercivity distribution and the vertical axis (H_u) reflects magnetostatic interactions [*Muxworthy and Williams*, 2005]. The plagioclase crystals exhibit a broad distribution extending to high H_c values with little spread in H_u values (Figure 4a), indicating that the exsolved magnetites are dominantly SD-like particles with minimal magnetostatic interactions [*Muxworthy and Williams*, 2005; *Egli et al.*, 2010]. Our FORC data do not exclude the possibility of nonuniform magnetization such as vortex states within a magnetite rod, as they could produce similar FORC diagrams [*Lappe et al.*, 2013].
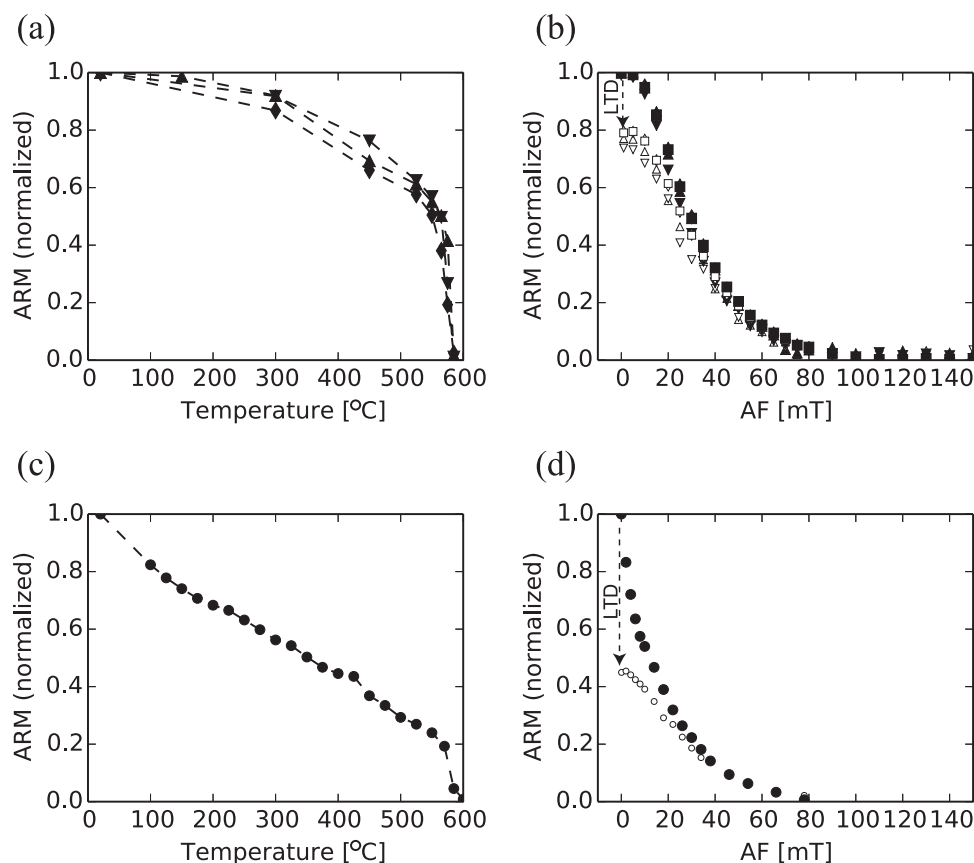
USUI ET AL.   116

Figure 2. ARM demagnetization of plagioclase crystals and a whole-rock sample. Remanence intensities are normalized to the intensities before demagnetization. (a) Thermal demagnetization of ARM of the single plagioclase crystals. (b) AF demagnetization of the ARM of the single plagioclase crystals (filled symbols). Open symbols represent the results of low-temperature demagnetization followed by AF demagnetization. (c) Thermal demagnetization of the ARM of the whole-rock sample. (d) AF demagnetization of the ARM of the whole-rock sample (filled symbols). Open symbols represent the results of low-temperature demagnetization followed by AF demagnetization.

The whole-rock sample exhibits low-coercivity and moderate magnetostatic interactions (Figures 3 and 4b). These features show that MD particles dominate the hysteresis properties of the whole-rock samples.
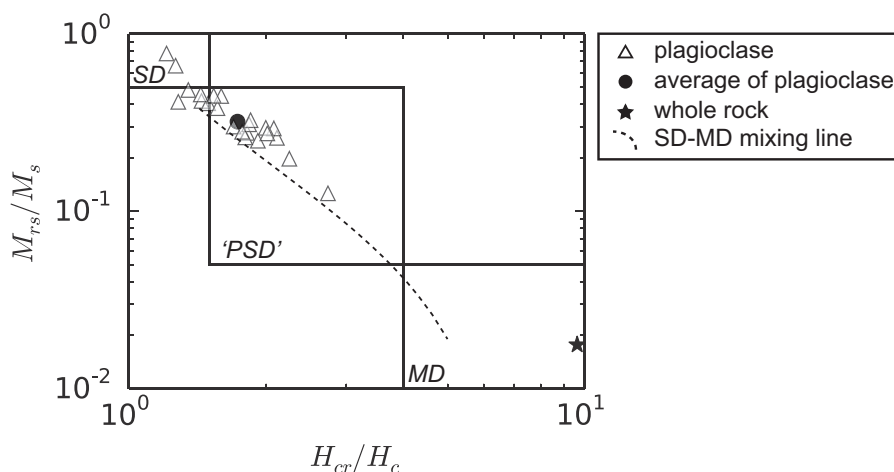

Figure 3. Hysteresis parameters represented in a Day plot. The single plagioclase crystals (open triangles) plot in the SD to "PSD" region. Two crystals exhibit $M_{rs}/M_s > 0.5$, and the remainder follow a theoretical mixing line between SD and MD end-members (dashed curve [*Dunlop*, 2002]). The average hysteresis parameters of the plagioclase crystals (filled circle) plot in the "PSD" field. The whole-rock sample (filled star) plots in the MD field.
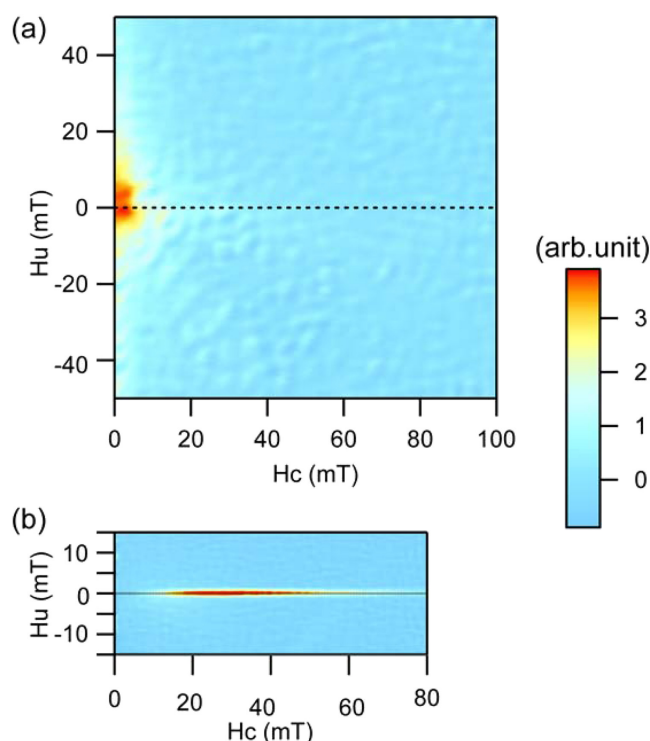
Figure 4. FORC diagrams showing the distribution of coercivity (H_c) and magnetostatic interactions (H_u). (a) The FORC diagram of the plagioclase crystals. (b) The FORC diagram of the whole-rock sample.

4.3. Remanence Anisotropy

The ARM anisotropy tensor estimates are summarized in Table 1 and Figure 5. The root mean square (RMS) of the least squares misfit is generally an order of magnitude smaller than the maximum and intermediate eigenvalues, but comparable to the minimum eigenvalue (Table 1), indicating a moderate error in the tensor estimates. The anisotropy degree is generally large with P_j ranging from 3.57 to 26.24. Most data show oblate anisotropy with the shape parameters T_j [*Jelinek*, 1981] ranging from −0.21 to 0.87. As the measured plagioclase crystals are not in regular shape, the anisotropy of sample shape may affect on the remanence anisotropy data, but we feel that the broad similarity in anisotropies among crystals indicate that the shape anisotropy is not a dominant factor.

4.4. TRM and ARM Acquisition

Figure 6 shows TRM and ARM acquisitions versus the applied DC field. The remanence intensities of TRM and ARM are normalized by isothermal remanent magnetization (IRM) imparted with a 2.7 T field using a pulse magnetizer Model 660 (2G Enterprises). All examined samples exhibit high efficiency of TRM acquisition and nonlinearity in the DC field of 10s of μT. The samples also exhibit high efficiency and nonlinearity of ARM acquisition. In contrast, the whole-rock sample exhibits low efficiency and linearity of ARM acquisition (Figure 6b).

5. Discussion

5.1. Occurrence of Exsolved Magnetite and Significance of Single Crystal Analysis

We report the first example of exsolved magnetite in silicate minerals in a Paleoarchean granitoid. The silicate minerals exhibit high magnetic stability (Figures 2 and 3), fulfilling the requirement of a good recorder of an ancient magnetic field. The FORC diagram of the plagioclase crystals exhibits a pronounced central ridge (Figure 4a), a feature favorable for Thellier paleointensity experiments [*Carvallo et al.*, 2006].

The minimal magnetostatic interactions inferred from our FORC analysis seem to be at odds with previous microscopic observations. A transmission electron microscopy study reported that some exsolved magnetite grains demonstrate internal exsolution of magnetite and ulvöspinel, forming an assemblage of magnetostatically interacting regions [*Feinberg et al.*, 2006]. *Wenk et al.* [2011] conducted energy-dispersive X-ray spectroscopy under a scanning electron microscope on exsolved oxides in plagioclases from a ~1.1 Ga anorthositic gneiss from the Adirondacks. They showed that some grains contain titanium as well as iron, but the distribution of the elements within a single oxide was not resolved. During slow cooling, titanomagnetite undergoes exsolution to magnetite and ulvöspinel [e.g., *Price*, 1980], so the detected titanium could reflect the ulvöspinel exsolution. Those microscopic studies, however, investigated a limited number of oxide grains. On the other hand, our FORC analysis indicates that the plagioclase crystals with numerous exsolved magnetite grains do not suffer from magnetostatic interactions as a whole. Minimal magnetostatic interactions were also reported for clinopyroxene [*Muxworthy and Evans*, 2013] and plagioclase crystals [*Usui*, 2013] from gabbroic rocks on the basis of the FORC diagrams of silicate crystals. It seems either that the internal exsolution of exsolved magnetite is not common, or that internal exsolution does not increase

Table 1. Summary of the Remanence Anisotropy of Single Plagioclase Crystals[a]

Sample Name	Mean ARM (nAm²)	w_1	w_2	w_3	RMS Misfit	P_j	T_j
PG157pl-a1	0.46	0.46	0.46	0.46	0.14	6.25	0.15
PG157pl-a2	1.31	1.31	1.31	1.31	0.09	4.44	0.34
PG157pl-a3	0.34	2.35	0.94	0.45	0.20	5.21	−0.11
PG157pl-a4	2.20	1.75	1.45	0.39	0.15	5.06	0.75
PG157pl-a5	1.05	2.05	1.38	0.35	0.14	6.35	0.55
PG157pl-a6	1.17	4.86	0.93	0.22	0.36	21.95	−0.07
PG157pl-a7	1.28	2.01	1.20	0.41	0.11	5.00	0.35
PG157pl-a8	0.66	2.31	1.65	0.26	0.17	10.40	0.69
PG157pl-a9	0.64	3.31	0.98	0.31	0.26	10.71	−0.03
PG157pl-a10	0.90	2.62	1.44	0.27	0.17	10.70	0.47
PG157pl-a11	0.46	1.92	1.08	0.48	0.14	4.00	0.17
PG157pl-a12	0.91	1.75	1.23	0.46	0.10	3.96	0.47
PG157pl-a13	0.44	1.69	1.26	0.47	0.12	3.83	0.54
PG157pl-a14	0.49	2.59	1.61	0.24	0.22	12.48	0.60
PG157pl-a15	0.27	1.79	1.11	0.51	0.13	3.57	0.24
PG157pl-a16	0.60	2.55	1.10	0.36	0.17	7.20	0.14
PG157pl-a17	1.15	4.28	0.83	0.28	0.33	15.46	−0.21
PG157pl-a18	1.15	1.82	1.24	0.44	0.13	4.32	0.46
PG157pl-a19	0.73	1.96	1.39	0.37	0.18	5.89	0.59
PG157pl-a20	0.69	2.27	1.49	0.29	0.13	8.65	0.59
PG157pl-a21	1.06	2.29	1.40	0.31	0.19	7.99	0.51
PG157pl-a22	1.34	2.25	1.24	0.36	0.13	6.52	0.35
PG157pl-a23	1.53	2.67	1.35	0.28	0.19	10.16	0.39
PG157pl-a24	1.27	2.12	1.25	0.38	0.18	5.85	0.39
PG157pl-a25	0.80	2.17	1.15	0.40	0.11	5.51	0.25
PG157pl-a26	1.18	2.76	1.00	0.36	0.13	7.64	0.01
PG157pl-a27	0.77	2.62	1.27	0.30	0.17	9.07	0.33
PG157pl-a28	1.65	2.34	1.11	0.38	0.12	6.15	0.17
PG157pl-a29	0.93	2.43	1.09	0.38	0.18	6.48	0.14
PG157pl-a30	1.36	2.16	1.45	0.32	0.17	7.53	0.59
PG157pl-a31	1.16	3.25	1.19	0.26	0.19	12.86	0.21
PG157pl-a32	0.61	1.98	1.27	0.40	0.09	5.26	0.44
PG157pl-a33	1.44	2.04	1.46	0.34	0.13	6.82	0.63
PG157pl-a34	2.62	2.10	1.27	0.37	0.10	5.90	0.42
PG157pl-a35	3.21	2.23	1.12	0.40	0.13	5.61	0.20
PG157pl-a36	3.14	1.96	1.38	0.37	0.11	5.81	0.58
PG157pl-a37	0.29	2.82	2.33	0.15	0.89	26.24	0.87
PG157pl-a38	0.48	1.93	1.11	0.47	0.62	4.18	0.21
PG157pl-a39	0.29	3.76	1.14	0.23	0.78	16.29	0.14
PG157pl-a40	1.34	1.97	1.31	0.39	0.52	5.47	0.50
Median		2.22	1.23	0.37			

[a]Mean ARM: mean ARM intensity at DC field of 70 μT calculated for the estimated tensor; w_1, w_2, and w_3: maximum, intermediate, and minimum eigenvalues (normalized by mean ARM), respectively; RMS misfit: normalized root mean square misfit of the least square tensor fitting; P_j and T_j: Jelinek's [1981] parameters.

the magnetostatic interactions to a significant degree. To resolve those two possibilities, more microscopic work is needed.

The magnetic measurements of the whole-rock samples appear to be ineffective in detecting exsolved magnetite. The whole-rock samples revealed low MDF, large low-temperature demagnetization (Figure 2d), and MD-like hysteresis properties (Figures 3 and 4b); these features are very different from the magnetic properties of silicate crystals with exsolved magnetite. The selective measurements of single silicate crystals revealed high remanence stability (Figure 2b) and SD-like hysteresis properties (Figures 3 and 4a). The high efficiency in ARM acquisition was also observed only in the plagioclase crystals and not in the whole rocks (Figure 6b). We emphasize that even a magnetically soft granitoid possibly contains silicates with exsolved magnetite, and single crystal measurements can effectively isolate the hidden signal of exsolved magnetite.

5.2. Averaging Out the Anisotropy Bias in Paleomagnetic Direction and Paleointensity

We quantified the ARM anisotropy tensors of 40 plagioclase crystals. These data enable the evaluation of the paleomagnetic recording bias of single plagioclase crystals containing exsolved magnetite. First, we consider the "typical" remanence anisotropy. The anisotropy data show a relatively large variation, ranging from 3.57 to 26.24 in P_j. We observe that P_j exhibits larger scatter for samples with smaller mean ARM
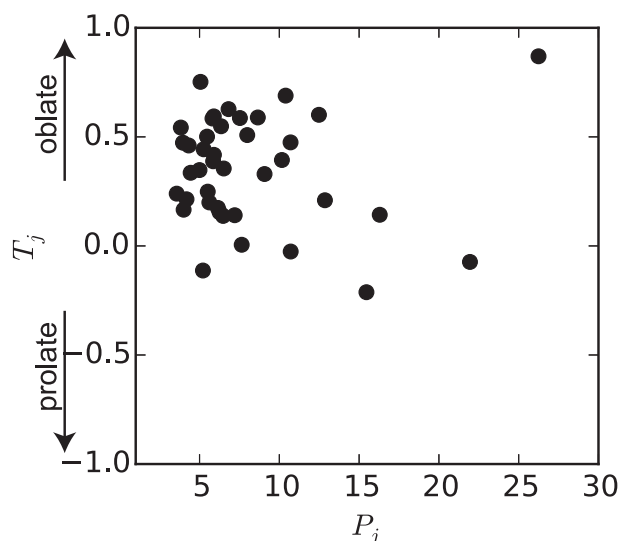
Figure 5. A Jelinek diagram showing the distribution of P_j and the shape parameter (T_j) of the ARM anisotropy tensors of the single plagioclase crystals.

(Figure 7), and samples with mean ARM larger than 1.5 nAm^2 exhibit consistent behavior with $P_j \sim 6$. This behavior may reflect the different abundance of different elongation directions of the exsolved magnetite. Microscopic observations revealed that the exsolved magnetite take four elongation directions with one being much more numerous (Figure 1f). If plagioclase crystals only contain exsolved magnetite with this direction, they would exhibit extremely high anisotropy. Addition of small number of exsolved magnetites with different elongation directions would produce large variation of anisotropy degree, and addition of sufficient number of such exsolved magnetites would result in moderate anisotropy with little variation and stronger remanence. For calculations, we used the median eigenvalues, $(w_1, w_2, w_3) = (2.22, 1.23, 0.37)$, to represent the typical remanence anisotropy of the plagioclase crystals with sufficient remanence intensity.

Theoretically, the magnetic remanence vector **M** and paleomagnetic field **H** are related through the remanence tensor K as: **M**=K**H**. In principle, the anisotropy bias can be corrected as: **H**=K^{-1}**M**. But, in practice, the determination of K always contains some experimental noise and this simple correction may not work well. For example, *Paterson* [2013] conducted phenomenological numerical simulations of paleointensity experiments, and concluded that the above correction should not be used for samples with $P_j > 3.5$. Because the plagioclase crystals exhibit much larger anisotropy, we investigated an alternative approach to cancel out the anisotropy bias by measuring a number of plagioclase crystals. This approach assumes that the whole rock is nearly isotropic. To evaluate the feasibility of this approach, we simulated the paleodirection and paleointensity estimates obtained from randomly oriented virtual crystals that have anisotropy eigenvalues of $(w_1, w_2, w_3) = (2.22, 1.23, 0.37)$.

The paleodirectional bias is simply defined as the angle between the external field and the acquired remanence, and this can be cancelled out by taking a simple arithmetic vector mean of the remanence direction. On the other hand, paleointensity simulation is more complicated and requires some explanation. Typical
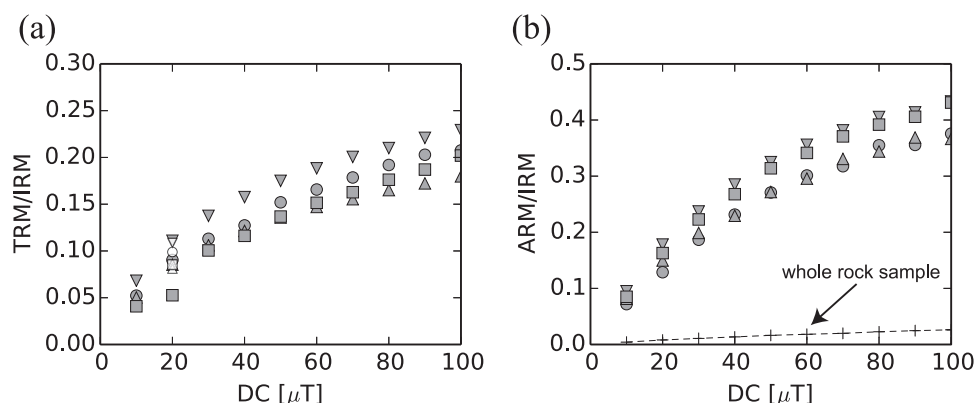

Figure 6. Acquisition of TRM and ARM. Remanence intensities are normalized by the IRM acquired in a 2.7 T field. Different plagioclase samples are distinguished by different symbols. (a) TRM acquisition against applied DC field showing nonlinearity. Open symbols represent an alteration check after all heating steps (see text for details). (b) ARM acquisition against applied DC field showing nonlinearity. Crosses represent the whole-rock sample.
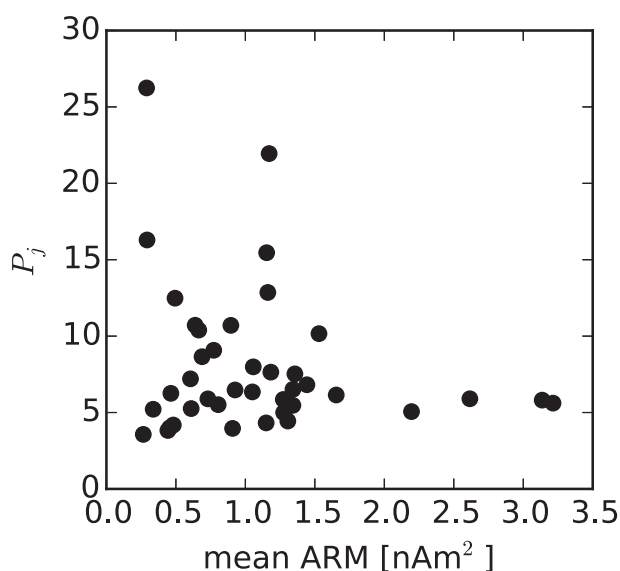
Figure 7. The correlation of the mean ARM and the corrected anisotropy degree (P_j). The larger variation in P_j at a smaller mean ARM implies that the measurement error affects the tensor parameters.

paleointensity experiments compare natural remanence ($[\mathbf{M}_{nrm}]_i$) and laboratory remanence ($[\mathbf{M}_{lab}]_i$), acquired in the ancient field ($\mathbf{H}_{nrm}$) and the laboratory field ($\mathbf{H}_{lab}$), respectively, with an assumption [e.g., *Dunlop and Özdemir*, 1997]:

$$||\mathbf{H}_{nrm}||/||[\mathbf{M}_{nrm}]_i|| = ||\mathbf{H}_{lab}||/||[\mathbf{M}_{lab}]_i||, \quad (1)$$

The subscript *i* denotes the remanence measured on one specific crystal. The paleointensity bias can be evaluated considering the distribution of the ratio of the magnitude of natural remanence to that of laboratory remanence:

$$r_i \equiv ||[\mathbf{M}_{nrm}]_i||/||[\mathbf{M}_{lab}]_i||. \quad (2)$$

For simplicity, we set $||\mathbf{H}_{lab}|| = ||\mathbf{H}_{nrm}||$, so that $r_i = 1$ in the absence of remanence anisotropy. In the presence of remanence anisotropy, remanences measured from multiple crystals form a series of random variables $\{||[\mathbf{M}_{nrm}]_i||\}$ and $\{||[\mathbf{M}_{lab}]_i||\}$. Because the probability distributions of $\{||[\mathbf{M}_{nrm}]_i||\}$ and $\{||[\mathbf{M}_{lab}]_i||\}$ are not standard distributions, the simple arithmetic mean of r_i would not converge to the true paleointensity. Indeed, numerical experiments showed that the simple arithmetic mean tends to overestimate the true paleointensity. To circumvent this problem, we consider the geometric mean of r_i. This would converge to the true paleointensity if the geometric means of $\{||[\mathbf{M}_{nrm}]_i\}$ and $\{||[\mathbf{M}_{lab}]_i||\}$ are the same. Since we assume the rock to be isotropic, the orientation of $\mathbf{H}_{nrm}$ is random with respect to the remanence anisotropy tensors of crystals within the rock. Suppose the orientation of $\mathbf{H}_{lab}$ to be random with respect to the remanence anisotropy tensor as well as to the orientation of $\mathbf{H}_{nrm}$. Then, $\{||[\mathbf{M}_{nrm}]_i||\}$ and $\{||[\mathbf{M}_{lab}]_i||\}$ become identically distributed random variables, and the geometric mean of $\{||[\mathbf{M}_{lab}]_i||\}$ is equal to the geometric mean of $\{||[\mathbf{M}_{nrm}]_i||\}$. In practice, this situation can be easily realized by measuring unoriented single crystals.

Figure 8 shows the results of the paleodirection simulations. To illustrate the bias, we present the bias in the individual measurements (Figure 8a). The bias in the average of a specific simulation is shown in Figure 8b, together with the bootstrap 95% confidence intervals for the average calculated by the 5000 simulations (Figure 8b). The confidence intervals show that individual measurements could contain a directional bias as large as 46° (Figure 8a). Averaging 20 crystals reduces the directional bias to ∼10°, and averaging 100 crystals reduces the bias to ∼5° for this specific example(Figure 8b). Note that, thanks to the strong remanence intensity of the exsolved magnetites, it is not difficult to acquire tens of crystals containing exsolved magnetites from a rock specimen.

The paleointensity simulations (Figure 9) lead to conclusions similar to those of the paleodirection simulations. The bias in individual measurements could be larger than a factor of 4 (Figure 9a), but averaging 20 crystals brings the estimate to within ∼30% of the true paleointensity (Figure 9b) for this specific example.

Note that the above calculation assumes ideal SD behavior to highlight the anisotropy effect. In actual experiments, factors such as non-SD behavior or experimental noise could reduce the effectiveness of the averaging. It is also expected that the number of crystals required to average out anisotropy bias would depend on remanence anisotropy, while remanence anisotropy of single silicate crystals containing exsolved magnetite is still poorly known. Comparison of our data with those of *Selkin et al*. [2014] indicates that anisotropy is variable among different rocks. Therefore, one should measure remanence anisotropy from target rocks to estimate the necessary number to average out the anisotropy effect.

To test the effect of averaging on paleointensity estimates from silicate crystals containing exsolved magnetites, we conducted paleointensity experiments to reconstruct laboratory-induced TRM taken as
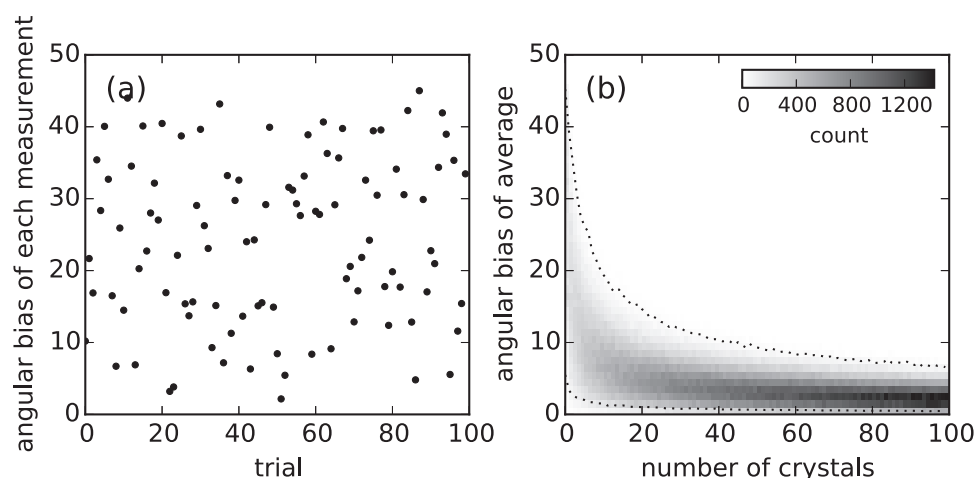
Figure 8. Numerical simulations of the directional bias due to magnetic anisotropy of virtual plagioclase crystals (see text for details). (a) Angular deviation of individual measurements in a single simulation. (b) Angular deviation for the mean remanence direction versus number of averaged crystals. For each number of crystals, 5000 simulations are conducted, and the results are plotted as histograms with 100 bins. Dashed lines represent the bootstrap 95% confidence limits calculated from 5000 simulations.

simulated natural remanent magnetization (NRM). We used 34 crystals from the Mount Edgar granite. The crystals are different from those used in the anisotropy experiments. Crystals were first heated to 600°C and cooled in a 20μT field using the custom made infrared heating apparatus to impart simulated NRM. Then, orientations of the crystals were changed randomly, and we impart TRM using a 20μT field. This is the same with the intensity of the magnetizing field for the simulated NRM; thus, the true paleointensity is given by $r = 1$. We took the ratio of the simulated NRM to total TRM as paleointensity estimates. The paleointensity estimates are summarized in Table 2. The geometric mean of r gives an estimate of r as $0.99(0.77 \sim 0.23)$, where the numbers in the parentheses represent the bootstrap 95% confidence interval. This indicates that the geometric mean recovers the true value of $r = 1$ well. In contrast, the arithmetic mean of r gives an estimate of the mean of r as $1.24(0.98 \sim 1.55)$, which overestimates the true value. These results agree with the numerical simulation.

5.3. Significance of the TRM and ARM Acquisition Characteristics on Paleointensity

Nonlinearity in TRM acquisition in an external field of a few tens of μT (Figure 6a) would invalidate the basic assumption of equation (1) in paleointensity experiments. *Selkin et al.* [2007] proposed to fit TRM acquisition using a hyperbolic tangent function as
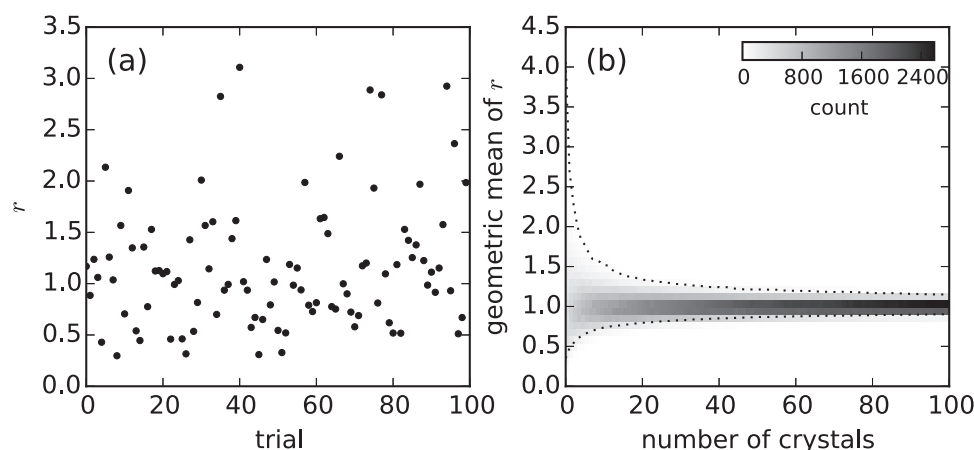

Figure 9. Numerical simulations of the paleointensity bias due to magnetic anisotropy of virtual plagioclase crystals (see text for details). (a) Paleointensity estimates of individual measurements, r, in a single simulation. (b) Paleointensity estimates from the geometric mean of r versus number of averaged crystals. For each number of crystals, 5000 simulations are conducted, and the results are plotted as histograms with 100 bins. Dashed lines represent the bootstrap 95% confidence limits calculated from 5000 simulations.

Table 2. Results of Paleointensity Simulation Experiments[a]

Sample	NRM (10^{-10} Am^2)	TRM (10^{-10} Am^2)	r
PG157-pl-ss-b	4.39	3.35	1.31
PG157-pl-ss-c2	2.49	1.71	1.46
PG157-pls-2	1.44	4.29	0.33
PG157-pls-3	1.95	1.12	1.74
PG157-pls-4	2.72	3.72	0.73
PG157-pls-5	3.50	2.49	1.40
PG157-pls-6	6.14	5.34	1.15
PG157-pls-7	2.88	2.75	1.05
PG157-pls-8	2.86	5.36	0.53
PG157-pls-9	0.97	1.48	0.66
PG157-pls-10	3.41	1.10	3.11
PG157-pls-11	3.23	0.92	3.52
PG157-pls-12	4.43	7.59	0.58
PG157-pls-13	0.92	3.80	0.24
PG157-pls-14	0.66	2.08	0.32
PG157-pls-15	12.94	8.74	1.48
PG157-pls-16	10.16	6.22	1.63
PG157-pls-17	3.74	3.61	1.04
PG157-pls-18	4.16	4.22	0.99
PG157-pls-19	1.87	1.31	1.42
PG157-pls-20	7.14	7.32	0.98
PG157-pls-21	9.30	6.03	1.54
PG157-pls-22	2.36	1.02	2.31
PG157-pls-23	0.81	3.47	0.23
PG157-pls-24	3.48	1.74	2.00
PG157-pls-25	1.95	3.00	0.65
PG157-pls-26	3.72	2.56	1.45
PG157-pls-27	15.15	4.94	3.06
PG157-pls-28	6.28	10.42	0.60
PG157-pls-29	3.60	5.18	0.69
PG157-pls-30	3.06	1.49	2.06
PG157-pls-31	2.42	5.01	0.48
PG157-pls-32	2.27	5.01	0.45
PG157-pls-33	4.53	4.49	1.01
Arthmetic mean			1.24
95% confidence interval (low)			0.98
95% confidence interval (high)			1.55
geometric mean			0.99
95% confidence interval (low)			0.77
95% confidence interval (high)			1.25

[a]95% confidence intervals were calculated by Bootstrap resampling.

$$M = c_1 \tanh(c_2 H), \qquad (3)$$

where M is TRM intensity, H is magnetic field intensity, and c_1 and c_2 are scaling constants. *Selkin et al.* [2007] also suggested that the nonlinear TRM acquisition can be corrected using the inverse of the hyperbolic tangent function. However, recent phenomenological paleointensity simulations by *Paterson* [2013] indicate that the correction is reasonable when H_{nrm} is not close to saturation (below 85% of the saturation) [*Paterson*, 2013]. The hyperbolic tangent fittings to our data indicate that the TRM of plagioclase crystals reaches near saturation at an applied field of 100 μT, and 85% of the saturation TRM corresponds to ∼50μT. Thus, we propose that the plagioclase crystals have sensitivity to the ancient field below 50 μT. If the ancient field was above 50 μT, TRM is too close to saturation, and the analysis of the plagioclase would be able to set only a lower bound for the ancient field intensity.

ARM normalization is sometimes utilized as a paleointensity technique without heating [e.g., *Banerjee and Mellema*, 1974]. Generally, ARM is thought to be less efficient than TRM at the same DC field, with ARM/IRM on the order of 0.01 and TRM/ARM of 1–4 [e.g., *Garrick-Bethell et al.*, 2009; *Yu*, 2010]. In contrast, ARM acquisition is very efficient in the exsolved magnetites studied here. The ARM/IRM was around 0.3 at a DC bias field of 50 μT (Figure 6b). *Cisowski* [1981] also reported efficient ARM acquisition of plagioclase from the Lambertville diabase [*Hargraves and Young*, 1969] with an ARM/IRM around 0.3 at a DC bias field of 200 μT. Similarly high ARM efficiency was reported from magnetotactic bacteria [e.g., *Pan et al.*, 2005] or pelagic sediments that possibly contain magnetofossils [e.g., *Yamazaki*, 2008]; the minimal interactions in magnetosomes or magnetofossils were considered to be the cause of the high ARM efficiency in those samples. We argue that the ARM acquisition characteristics are the sign of minimal magnetostatic interactions among the exsolved magnetites. The plagioclase crystals show a TRM/ARM ratio of ∼0.4 with an ARM larger than the TRM. This reinforces the claim that ARM acquisition depends critically on grain size and concentration, and that ARM normalization should be used with caution [*Bailey and Dunlop*, 1977].

6. Conclusions

We found tiny exsolved magnetite in plagioclase from a Paleoarchean granitoid in the Mount Edgar Complex. Single plagioclase crystal measurements revealed that the exsolved magnetites are in near-SD state with minimal magnetostatic interactions; thus, they have the potential to preserve reliable paleomagnetic information for billions of years.

Plagioclase single crystals exhibit high ARM anisotropy with median eigenvalues of 40 plagioclase crystals of ($w1$, $w2$, $w3$) = (2.22, 1.23, 0.37). For single silicate paleomagnetism using exsolved magnetites, it is

necessary to average multiple crystals to mitigate the bias due to anisotropy. Using a numerical calculation and simulated paleointensity experiments, we conclude that, for the plagioclases studied here, averaging a few tens of crystals is predicted to reduce the directional bias below 10° and paleointensity bias below 30%. The same procedure would be applicable to the single silicate crystal measurements targeting exsolved magnetite. TRM acquisition of the plagioclase crystals exhibits nonlinearity at DC fields of a few tens of μT. Following the results of Paterson [2013], this behavior would limit the use of plagioclase crystals in paleointensity experiment to the case where H_{nrm} is below 50 μT. Above this field, the plagioclase crystals would be able to set the lower bound of the paleointensity. The TRM/ARM ratio of the plagioclase crystals is $\sim$0.4 for the same DC field, distinctively lower than for other natural samples [e.g., *Yu*, 2010; *Garrick-Bethell et al.*, 2009]. Paleointensity experiments with ARM normalization applied to magnetic minerals such as exsolved magnetite should be carried out with caution.

Although exsolved magnetites in silicate are not frequently reported from granitoid, they may not be rare. In our sample, the magnetic properties of the whole rock do not reflect the presence of the exsolved magnetite. Microscopic observations and selective single crystal measurements are essential to detect the presence of exsolved magnetite and to isolate the paleomagnetic information carried by them.

References

Bailey, M. E., and D. J. Dunlop (1977), On the use of anhysteretic remanent magnetization in paleointensity determination, *Phys. Earth Planet. Inter.*, *13*(4), 360–362.

Banerjee, S., and J. Mellema (1974), A new method for the determination of paleointensity from the A.R.M. properties of rocks, *Earth Planet. Sci. Lett.*, *23*(2), 177–184.

Borradaile, G. J., and M. Stupavsky (1995), Anisotropy of magnetic susceptibility: Measurement schemes, *Geophys. Res. Lett.*, *22*(15), 1957–1960.

Carvallo, C., A. P. Roberts, R. Leonhardt, C. Laj, C. Kissel, M. Perrin, and P. Camps (2006), Increasing the efficiency of paleointensity analyses by selection of samples using first-order reversal curve diagrams, *J. Geophys. Res.*, *111*, B12103, doi:10.1029/2005JB004126.

Cisowski, S. (1981), Interacting vs. non-interacting single domain behavior in natural and synthetic samples, *Phys. Earth Planet. Inter.*, *26*(1), 56–62.

Coe, R. S. (1979), The effect of shape anisotropy on TRM direction, *Geophys. J. Int.*, *56*(2), 369–383.

Collins, W., and C. Gray (1990), Rb-Sr isotopic systematics of an Archaean granite–gneiss terrain: The Mount Edgar Batholith, Pilbara block, western Australia, *Aust. J. Earth Sci.*, *37*(1), 9–22.

Davies, K. E. (1981), Magnetite rods in plagioclase as the primary carrier of stable nrm in ocean floor gabbros, *Earth Planet. Sci. Lett.*, *55*(1), 190–198.

Day, R., M. Fuller, and V. Schmidt (1977), Hysteresis properties of titanomagnetites: Grain-size and compositional dependence, *Phys. Earth Planet. Inter.*, *13*(4), 260–267.

Dodson, M. H., and E. McClelland-Brown (1980), Magnetic blocking temperatures of single-domain grains during slow cooling, *J. Geophys. Res.*, *85*(B5), 2625–2637.

Dunlop, D. J. (2002), Theory and application of the day plot (Mrs/Ms versus Hcr/Hc): 1. Theoretical curves and tests using titanomagnetite data, *J. Geophys. Res.*, *107*(B3), doi:10.1029/2001JB000486.

Dunlop, D. J. and Ö. Özdemir (1997), *Rock Magnetism: Fundamentals and Frontiers*, Cambridge Univ. Press, Cambridge, U. K.

Dunlop, D. J., B. Zhang and Ö. Özdemir (2005), Linear and nonlinear Thellier paleointensity behavior of natural minerals, *J. Geophys. Res.*, *110*, B01103, doi:10.1029/2004JB003095.

Egli, R., A. P. Chen, M. Winklhofer, K. P. Kodama, and C.-S. Horng (2010), Detection of noninteracting single domain particles using first-order reversal curve diagrams, *Geochem. Geophys. Geosyst.*, *11*, Q01Z11, doi:10.1029/2009GC002916.

Evans, M., and M. McElhinny (1966), The paleomagnetism of the Modipe Gabbro, *J. Geophys. Res.*, *71*(24), 6053–6063.

Evans, M., M. McElhinn, and A. C. Gifford (1968), Single domain magnetite and high coercivities in a gabbroic intrusion, *Earth Planet. Sci. Lett.*, *4*(2), 142–146.

Feinberg, J. M., H.-R. Wenk, P. R. Renne, and G. R. Scott (2004), Epitaxial relationships of clinopyroxene-hosted magnetite determined using electron backscatter diffraction (EBSD) technique, *Am. Mineral.*, *89*(2-3), 462–466.

Feinberg, J. M., G. R. Scott, P. R. Renne, and H.-R. Wenk (2005), Exsolved magnetite inclusions in silicates: Features determining their remanence behavior, *Geology*, *33*(6), 513–516.

Feinberg, J. M., R. J. Harrison, T. Kasama, R. E. Dunin-Borkowski, G. R. Scott, and P. R. Renne (2006), Effects of internal mineral structures on the magnetic remanence of silicate-hosted titanomagnetite inclusions: An electron holography study, *J. Geophys. Res.*, *111*, B12S15, doi: 10.1029/2006JB004498.

Fleet, M. E., G. A. Bilcox, and R. L. Barnett (1980), Oriented magnetite inclusions in pyroxenes from the Grenville province, *Can. Mineral.*, *18*(1), 89–99.

Garrick-Bethell, I., B. P. Weiss, D. L. Shuster, and J. Buz (2009), Early lunar magnetism, *Science*, *323*(5912), 356–359.

Gee, J., and W. Meurer (2002), Slow cooling of middle and lower oceanic crust inferred from multicomponent magnetizations of gabbroic rocks from the Mid-Atlantic ridge south of the Kane fracture zone (MARK) area, *J. Geophys. Res.*, *107*(B7), doi:10.1029/2000JB000062.

Halgedahl, S. L., and R. D. Jarrard (1995), Low-temperature behavior of single-domain through multidomain magnetite, *Earth Planet. Sci. Lett.*, *130*(1), 127–139.

Halgedahl, S. L., R. Day, and M. Fuller (1980), SThe effect of cooling rate on the intensity of weak-field TRM in single-domain magnetite, *J. Geophys. Res.*, *85*(B7), 3690–3698.

Hargraves, R., and W. Young (1969), Source of stable remanent magnetism in Lambertville diabase, *Am. J. Sci.*, *267*(10), 1161–1177.

Harrison, R. J., and J. M. Feinberg (2008), FORCinel: An improved algorithm for calculating first-order reversal curve distributions using locally weighted regression smoothing, *Geochem. Geophys. Geosyst.*, *9*, Q05016, doi:10.1029/2008GC001987.

Jelinek, V. (1981), Characterization of the magnetic fabric of rocks, *Tectonophysics*, *79*(3), T63–T67.

Lagroix, F., and G. J. Borradaile (2000), Magnetic fabric interpretation complicated by inclusions in mafic silicates, *Tectonophysics*, *325*(3), 207–225.

Lappe, S.-C. L. L., J. M. Feinberg, A. Muxworthy, and R. J. Harrison (2013), Comparison and calibration of nonheating paleointensity methods: A case study using dusty olivine, *Geochem. Geophys. Geosyst.*, *14*, 2143–2158, doi:10.1002/ggge.20141.

Layer, P. W., A. Kröner, and M. McWilliams (1996), An Archean geomagnetic reversal in the Kaap Valley pluton, South Africa, *Science*, *273*(5277), 943–946.

Muxworthy, A., and M. Evans (2013), Micromagnetics and magnetomineralogy of ultrafine magnetite inclusions in the Modipe Gabbro, *Geochem. Geophys. Geosyst.*, *14*, 921–928, doi:10.1029/2012GC004445.

Muxworthy, A., and W. Williams (2005), Magnetostatic interaction fields in first-order-reversal-curve diagrams, *J. Appl. Phys.*, *97*(6), 063905.

Muxworthy, A., M. Evans, S. Scourfield, and J. King (2013), Paleointensity esults from the late-Archaean Modipe Gabbro of Botswana, *Geochem. Geophys. Geosyst.*, *14*, 2198–2205, doi:10.1002/ggge.20142.

Nye, J. F. (1957), *Physical Properties of Crystals: Their Representation by Tensors and Matrices*, Oxford Univ. Press, Oxford, U. K.

Pan, Y., N. Petersen, M. Winklhofer, A. F. Davila, Q. Liu, T. Frederichs, M. Hanzlik, and R. Zhu (2005), Rock magnetic properties of uncultured magnetotactic bacteria, *Earth Planet. Sci. Lett.*, *237*(3), 311–325.

Paterson, G. A. (2013), The effects of anisotropic and non-linear thermoremanent magnetizations on thellier-type paleointensity data, *Geophys. J. Int.*, *193*(2), 694–710.

Pike, C. R., A. P. Roberts, and K. L. Verosub (1999), Characterizing interactions in fine magnetic particle systems using first order reversal curves, *J. Appl. Phys.*, *85*(9), 6660–6667.

Price, G. (1980), Exsolution microstructures in titanomagnetites and their magnetic significance, *Phys. Earth Planet. Inter.*, *23*(1), 2–12.

Renne, P. R., G. R. Scott, J. M. Glen, and J. M. Feinberg (2002), Oriented inclusions of magnetite in clinopyroxene: Source of stable remanent magnetization in gabbros of the Messum Complex, Namibia, *Geochem. Geophys. Geosyst.*, *3*(12), 1079, doi:10.1029/2002GC000319.

Roberts, A. P., C. R. Pike, and K. L. Verosub (2000), First-order reversal curve diagrams: A new tool for characterizing the magnetic properties of natural samples, *J. Geophys. Res.*, *105*(B12), 28,461–28,475.

Selkin, P., J. Gee, L. Tauxe, W. Meurer, and A. Newell (2000), The effect of remanence anisotropy on paleointensity estimates: A case study from the Archean Stillwater Complex, *Earth Planet. Sci. Lett.*, *183*(3), 403–416.

Selkin, P., J. Gee, W. Meurer, and S. Hemming (2008), Paleointensity record from the 2.7 ga Stillwater Complex, Montana, *Geochem. Geophys. Geosyst.*, *9*, Q12023, doi:10.1029/2008GC001950.

Selkin, P. A., J. S. Gee, and L. Tauxe (2007), Nonlinear thermoremanence acquisition and implications for paleointensity data, *Earth Planet. Sci. Lett.*, *256*(1), 81–89.

Selkin, P. A., J. S. Gee, and W. P. Meurer (2014), Magnetic anisotropy as a tracer of crystal accumulation and transport, Middle Banded Series, Stillwater Complex, Montana, *Tectonophysics*, *629*, 123–137.

Sims, J. P., and J. L. Carson (2001), The Geology of the Mound Edgar and Corunna Downs Igneous Complexes, East Pilbara Craton, Western Australia, AGSO Geoscience Australia, Canberra, Australia.

Sobolev, P. (1990), Orientation of acicular iron-ore mineral inclusions in plagioclase, *Int. Geol. Rev.*, *32*(6), 616–628.

Tarduno, J., R. Cottrell, and A. Smirnov (2006), The paleomagnetism of single silicate crystals: Recording geomagnetic field strength during mixed polarity intervals, superchrons, and inner core growth, *Rev. Geophys.*, *44*, RG1002, doi:10.1029/2005RG000189.

Tarduno, J. A., R. D. Cottrell, M. K. Watkeys, and D. Bauch (2007), Geomagnetic field strength 3.2 billion years ago recorded by single silicate crystals, *Nature*, *446*(7136), 657–660.

Tarduno, J. A., R. D. Cottrell, M. K. Watkeys, A. Hofmann, P. V. Doubrovine, E. E. Mamajek, D. Liu, D. G. Sibeck, L. P. Neukirch, and Y. Usui (2010), Geodynamo, solar wind, and magnetopause 3.4 to 3.45 billion years ago, *Science*, *327*(5970), 1238–1240.

Tarduno, J. A., E. Blackman, and E. E. Mamajek (2014), Detecting the oldest geodynamo and attendant shielding from the solar wind: Implications for habitability, *Phys. Earth Planet. Inter.*, *233*, 68–87.

Usui, Y. (2013), Paleointensity estimates from oceanic gabbros: Effects of hydrothermal alteration and cooling rate, *Earth Planets Space*, *65*(9), 985–996.

Usui, Y., and N. Nakamura (2009), Nonlinear thermoremanence corrections for thellier paleointensity experiments on single plagioclase crystals with exsolved magnetites: a case study for the Cretaceous normal superchron, *Earth Planets Space*, *61*(12), 1327–1337.

Usui, Y., N. Nakamura, and T. Yoshida (2006), Magnetite microexsolutions in silicate and magmatic flow fabric of the Goyozan granitoid (NE Japan): Significance of partial remanence anisotropy, *J. Geophys. Res.*, *111*, B11101, doi:10.1029/2005JB004183.

Usui, Y., J. A. Tarduno, M. Watkeys, A. Hofmann, and R. D. Cottrell (2009), Evidence for a 3.45-billion-year-old magnetic remanence: Hints of an ancient geodynamo from conglomerates of South Africa, *Geochem. Geophys. Geosyst.*, *10*, Q09Z07, doi:10.1029/2009GC002496.

Uyeda, S., M. Fuller, J. Belshe, and R. Girdler (1963), Anisotropy of magnetic susceptibility of rocks and minerals, *J. Geophys. Res.*, *68*(1), 279–291.

Wenk, H.-R., K. Chen, and R. Smith (2011), Morphology and microstructure of magnetite and ilmenite inclusions in plagioclase from Adirondack anorthositic gneiss, *Am. Mineral.*, *96*(8-9), 1316–1324.

Williams, I., and W. Collins (1990), Granite-greenstone terranes in the Pilbara block, Australia, as coeval volcano-plutonic complexes; evidence from U-Pb zircon dating of the Mount Edgar Batholith, *Earth Planet. Sci. Lett.*, *97*(1), 41–53.

Windley, B. F., and D. Bridgwater (1971), The evolution of Archaean low-and high grade terrains, *Geol. Soc. Aust. Spec. Publ.*, *3*, 33–46.

Yamazaki, T. (2008), Magnetostatic interactions in deep-sea sediments inferred from first-order reversal curve diagrams: Implications for relative paleointensity normalization, *Geochem. Geophys. Geosyst.*, *9*, Q02005, doi:10.1029/2007GC001797.

Yoshihara, A., and Y. Hamano (2004), Paleomagnetic constraints on the Archean geomagnetic field intensity obtained from komatiites of the Barberton and Belingwe greenstone belts, South Africa and Zimbabwe, *Precambrian Res.*, *131*(1), 111–142.

Yu, Y. (2010), Paleointensity determination using anhysteretic remanence and saturation isothermal remanence, *Geochem. Geophys. Geosyst.*, *11*, Q02Z12, doi:10.1029/2009GC002804.